Synthesis, structure, and electronic properties of tris(propane-1,3-dithiolato) and tris(ethylene-1,2-dithiolato) complexes of niobium(V) and tantalum(V)

ARTICLE *in* INORGANIC CHEMISTRY · FEBRUARY 1989

Impact Factor: 4.76 · DOI: 10.1021/ic00303a032

5 AUTHORS, INCLUDING:

Carlo Mealli
Italian National Research Council
245 PUBLICATIONS **5,041** CITATIONS

SEE PROFILE

Contribution from the Department of Macromolecular Science, Faculty of Science, Osaka University, Toyonaka, Osaka 560, Japan, and Istituto per lo Studio della Stereochimica ed Energetica dei Composti di Coordinazione CNR, 50132 Firenze, Italy

Synthesis, Structure, and Electronic Properties of Tris(propane-1,3-dithiolato) and Tris(ethylene-1,2-dithiolato) Complexes of Niobium(V) and Tantalum(V)

Kazuyuki Tatsumi,*,† Ichiro Matsubara,† Yoitsu Sekiguchi,† Akira Nakamura,*,† and Carlo Mealli‡

Received June 14, 1988

The synthesis and spectroscopic studies of $[A][M(SCH_2CH_2CH_2S)_3]$ and $[A][M(SCH{=}CHS)_3]$ (A = Ph_4P, Et_4N; M = Nb, Ta) and the crystal structure of $[Ph_4P][Nb(SCH_2CH_2CH_2S)_3]$ are presented. Analysis of the IR and Raman spectra of these species as well as of the analogous ethanedithiolate complexes $[A][M(SCH_2CH_2S)_3]$ reveals that the degree of trigonal twist of the MS_6 polyhedron varies in a complicated fashion depending on minute perturbation of crystal-packing forces and electronic factors. Of them the ethylenedithiolate complexes have a geometry closest to the trigonal-prismatic limit. Electronic properties of the dithiolate complexes are examined in terms of CV and electronic spectra and extended Hückel calculations.

Introduction

One of our recent interests has been to explore the chemistry of dithiolate complexes of group 5 transition metals.[1-3] We reported syntheses of the homoleptic ethane-1,2-dithiolate complexes of Nb and Ta, and the X-ray structure analysis of $[Et_4N][Nb(SCH_2CH_2S)_3]$ revealed that the NbS_6 core had a geometry midway between the octahedral and trigonal-prismatic limits.[1b,4] Subsequently these ethane-1,2-dithiolate complexes were found to undergo an unusual rearrangement, via a C–S bond cleavage and a following bond recombination, giving $[MS(SCH_2CH_2S)(SCH_2CH_2SCH_2CH_2S)]^-$ (M = Nb, Ta) in good yield in the presence of a trace amount of water, methanol, phenol, etc.[1c,d]

To provide further information concerning the structure and chemical/physical properties of such simple tris(dithiolate) complexes, we have extended our study to those with propane-1,3-dithiolate and ethylene-1,2-dithiolate complexes. This paper reports the detailed synthesis of $[A][M(SCH_2CH_2CH_2S)_3]$ and $[A][M(SCH{=}CHS)_3]$ together with that of $[A][M(SCH_2CH_2S)_3]$ (A = Ph_4P, Et_4N; M = Nb, Ta), their characterization in terms of IR, Raman, CV, and electronic spectra, and the X-ray structure analysis of $[Ph_4P][Nb(SCH_2CH_2CH_2S)_3]$. The IR and Raman spectra are interpreted with the aid of Urey–Bradley type force field analysis, providing us with geometrical information about the MS_6 polyhedron. Further, we discuss the results of CV and electronic spectra using extended

Chart I

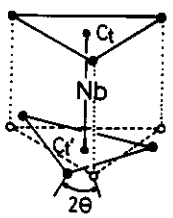

Hückel calculations on $[Nb(SCH_2CH_2S)_3]^-$ and $[Nb(SCH{=}CHS)_3]^-$.

† Osaka University.
‡ Istituto per lo Studio della Stereochimica ed Energetica dei Composti di Coordinazione.

(1) (a) Tatsumi, K.; Takeda, J.; Sekiguchi, Y.; Kohsaka, M.; Nakamura, A. *Angew. Chem.* **1985**, *97*, 355–356; *Angew. Chem., Int. Ed. Engl.* **1985**, *24*, 332–333. (b) Tatsumi, K.; Sekiguchi, Y.; Nakamura, A.; Cramer, R. E.; Rupp, J. J. *Angew. Chem.* **1986**, *98*, 95–96; *Angew. Chem., Int. Ed. Engl.* **1986**, *25*, 86–87. (c) Tatsumi, K.; Sekiguchi, Y.; Nakamura, A.; Cramer, R. E.; Rupp, J. J. *J. Am. Chem. Soc.* **1986**, *108*, 1358–1359. (d) Tatsumi, K.; Sekiguchi, Y.; Kohsaka, M.; Sebata, M.; Nakamura, A.; Cramer, R. E.; Rupp, J. J. To be submitted for publication. (e) Tatsumi, K.; Sekiguchi, Y.; Sebata, M.; Nakamura, A.; Cramer, R. E.; Chung, T. *Angew. Chem.*, in press.
(2) Elegant studies of tris(benzene-1,2-dithiolato) and tris(toluene-3,4-dithiolato) complexes of Nb and Ta and those of other early transition metals are available: (a) Bennett, M. J.; Cowie, M.; Martin, J. L.; Takats, J. *J. Am. Chem. Soc.* **1973**, *95*, 7504–7505. (b) Martin, J. L.; Takats, J. *Inorg. Chem.* **1975**, *14*, 73–78, 1358–1364. (c) Cowie, M.; Bennett, M. J. *Inorg. Chem.* **1976**, *15*, 1584–1589, 1589–1595, 1595–1603.
(3) Synthesis of $Cp_2Nb(SCR{=}CRS)^+$ (R = Me, Ph) has appeared: Viard, B.; Amaudrut, J.; Sala-Pala, J.; Fakhr, A.; Mugnier, Y.; Moise, C. *J. Organomet. Chem.* **1985**, *292*, 403–409.

0020-1669/89/1328-0773$01.50/0

Experimental Section

Preparation of Compounds. All operations and manipulations were performed under an argon atmosphere with Schlenk-type glassware. Solvents were distilled (CH_3CN and CH_2Cl_2 from CaH_2; DMF from the benzene azeotrope and then from BaO) under argon. Deuteriated solvents were trap-to-trap-distilled from CaH_2. Melting points (decomposition) are uncorrected.

Reagents were obtained as follows: *cis*-$CH(SCH_2Ph)$=$CH(SCH_2Ph)$, prepared from *cis*-CHCl=CHCl, $PhCH_2Cl$, and $SC(NH_2)_2$ by a literature procedure;[5] $HSCH_2CH_2CH_2SH$ (Aldrich), distilled from CaH_2 before use; $LiSCH_2CH_2CH_2SLi$, prepared from $HSCH_2CH_2CH_2SH$ and *n*-BuLi.

Preparation of LiSCH=CHSLi. Into a three-necked flask containing 34.9 g (0.128 mol) of *cis*-$CH(SCH_2Ph)$=$CH(SCH_2Ph)$ and 1.7 g (0.25 mol) of lithium was introduced NH_3 gas at −78 °C until ca. 300 mL of liquid NH_3 was stored. After the NH_3 solution became orange, the liquid NH_3 was evaporated and the residue was washed with 5:1, 3:1, 1:1, and then 1:5 C_6H_6/CH_3CN solution (v/v) until the filtrate was nearly colorless to yield 4.6 g (0.044 mol) of LiSCH=CHSLi.

Preparation of $[Ph_4P][Nb(SCH_2CH_2CH_2S)_3]$ (1a). A CH_3CN solution (50 mL) of $NbCl_5$ (4.8 g, 18 mmol) was added dropwise to a slurry of $LiSCH_2CH_2CH_2SLi$ (6.8 g, 57 mmol) in CH_3CN (60 mL) with stirring at 0 °C. The reaction mixture was allowed to warm up to room temperature and stirred at this temperature for 2 h. The solution turned from pale yellow to brown. After insoluble materials were filtered off, a CH_3CN solution (40 mL) of Ph_4PBr (6.0 g, 14 mmol) was slowly added to the filtrate, and **1a** precipitated out as an orange-red crystalline powder (yield 43%). Recrystallization from DMF gave orange-red crystals (recovery 70%) that were suitable for the X-ray analysis; mp 65 °C dec. ^1H NMR ($CDCl_3$, 100 MHz; room temperature): δ 7.8 (m, 20 H, Ph_4P), 3.50 (t, J = 7 Hz, 12 H, $SCH_2CH_2CH_2S$), 1.82 (quintet, J = 7 Hz, 6 H, $SCH_2CH_2CH_2S$). UV–visible (λ_{max}, nm (ϵ_{max}, M^{-1} cm^{-1}), CH_3CN): 348 (15 000), 407 (12 000), ~470 sh. Anal. Calcd for $C_{33}H_{38}S_6PNb$: C, 52.78; H, 5.10; S, 25.62. Found: C, 52.45; H, 5.11; S, 25.18.

The following three tris(propanedithiolato) complexes were synthesized by a procedure similar to that described above for **1a**.

$[Et_4N][Nb(SCH_2CH_2CH_2S)_3]$ (1b). The reaction system $NbCl_5$ (2.7 g, 10 mmol), $LiSCH_2CH_2CH_2SLi$ (3.8 g, 32 mmol), and Et_4NCl (1.6 g, 10 mmol) in CH_3CN gave spectroscopically pure **1b** as an orange-red crystalline powder (yield 75%), mp 51 °C dec. ^1H NMR (CD_3CN, 100 MHz): δ 3.46 (t, J = 6 Hz, 12 H, $SCH_2CH_2CH_2S$), 3.19 (q, J = 7 Hz, 8 H, NCH_2CH_3), 1.87 (quintet, J = 6.5 Hz, 6 H, $SCH_2CH_2CH_2S$), 1.24 (tt, J_{HH} = 7 Hz, 12 H, NCH_2CH_3). UV–visible (λ_{max}, nm (ϵ, M^{-1} s^{-1}), CH_3CN): 277 (14 000), 344 (15 000), 403 (11 000), ~480 sh.

$[Ph_4P][Ta(SCH_2CH_2CH_2S)_3]$ (2a). The reaction system $TaCl_5$ (3.6 g, 10 mmol), $LiSCH_2CH_2CH_2SLi$ (4.7 g, 39 mmol), and Ph_4PBr (3.8 g, 9.1 mmol) in CH_3CN gave a yellow crystalline powder of **2a** (yield 75%), which was then recrystallized from DMF to give analytically pure **2a** (recovery 80%), mp 63 °C dec. ^1H NMR ($CDCl_3$, 100 MHz): δ 7.8 (m, 20 H, Ph_4P), 3.83 (t, J = 6.5 Hz, 12 H, $SCH_2CH_2CH_2S$), 1.76 (quintet, J = 6.5 Hz, 6 H, $SCH_2CH_2CH_2S$). UV–visible (λ_{max}, nm (ϵ, M^{-1} s^{-1}), CH_3CN): 267 (15 000), 273 (13 000), 307 (12 000), 352 (12 000), ~400 sh. Anal. Calcd for $C_{33}H_{38}S_6PTa$: C, 47.25; H, 4.57; S, 22.93. Found: C, 47.07; H, 4.56; S, 22.60.

$[Et_4N][Ta(SCH_2CH_2CH_2S)_3]$ (2b). The reaction system $TaCl_5$ (3.7 g, 10.3 mmol), $LiSCH_2CH_2CH_2SLi$ (4.7 g, 38.9 mmol), and Et_4NCl (1.6 g, 9.7 mmol) in CH_3CN gave spectroscopically pure **2b** as a yellow crystalline powder (yield 83%); mp 62 °C dec. ^1H NMR (DMF-d_7, 100 MHz): δ 3.44 (t, J = 6 Hz, 12 H, $SCH_2CH_2CH_2S$), 3.14 (q, J = 7 Hz, 8 H, NCH_2CH_3), 1.40 (quintet, J = 6 Hz, 6 H, $SCH_2CH_2CH_2S$), 1.02 (tt, J_{HH} = 7 Hz, 12 H, NCH_2CH_3). UV–visible (CH_3CN): 263 (9100), 306 (10 000), 350 (11 000), ~400 sh.

Table I. Summary of Crystallographic Data for **1a**

formula	$C_{33}H_{38}S_6PNb$
mol wt	750.9
a, Å	14.118 (7)
b, Å	9.735 (6)
c, Å	12.755 (6)
β, deg	91.5 (9)
cryst syst	monoclinic
Z	2
V, Å^3	1752
d_{calcd}, g/cm^3	1.423
space group	Pn
cryst dimens, mm	0.15 × 0.12 × 0.10
F(000), e	790.0
abs coeff, μ cm^{-1}	6.90 (Mo Kα)
scan speed, deg/min	0.06 (ω–2θ scan)
scan range, deg	1.0 below Kα_1 to 1.0 above Kα_2
2θ limits, deg	$5 \le 2\theta \le 50$
no. of data collected	3419
no. of obsd data ($F_o^2 > 3\sigma(F_o^2)$)	2256
no. of variables	202
R (R_w),[a] %	6.42 (6.51)

[a] $R = \sum(|F_o| - |F_c|)/\sum|F_o|$ and $R_w = [\sum w(|F_o| - |F_c|)^2/\sum wF_o^2]^{1/2}$, where $w = 1.0(\sigma(F)^2 + 0.005|F_o|^2)^{-1}$.

Preparation of $[Ph_4P][Nb(SCH{=}CHS)_3]$ (3a). To a CH_3CN suspension (40 mL) of LiSCH=CHSLi (3.2 g, 30.8 mmol) was added dropwise a CH_3CN solution (25 mL) of $NbCl_5$ (2.2 g, 8.1 mmol) at 0 °C. The reaction mixture was stirred for 2 h, after which the solvent was removed in vacuo. Then the residue was dissolved in CH_2Cl_2 (130 mL) and the carmine-colored solution was filtered to remove LiCl. To this filtrate was added a CH_2Cl_2 solution of Ph_4PBr (3.35 g, 8.0 mmol), and the solution was concentrated in vacuo to ca. one-fifth of its original volume. A deep dull purple powder (**3a**) precipitated. Further concentration of the remaining solution gave another precipitate of **3a**, which was collected by filtration and washed with 1:9 CH_3CN/Et_2O (v/v) and then with Et_2O. The precipitates were combined and recrystallized from CH_2Cl_2 to give a crystalline powder (yield 39%), mp 179–184 °C dec. ^1H NMR (DMSO-d_6, 100 MHz): δ 7.79 (s, 6 H, $SCH{=}CHS$), 7.60–8.12 (m, 20 H, Ph_4P). UV–visible (λ_{max}, nm (ϵ, M^{-1} cm^{-1}), CH_3CN): 317 (1200), 410 (3000), 462 (2600), 556 (2800). Anal. Calcd for $C_{30}H_{26}PS_6Nb$: C, 51.27; H, 3.74; S, 27.37. Found: C, 51.10; H, 3.85; S, 26.91.

The following Et_4N^+ salts of tris(ethylenedithiolato) complexes were synthesized by a procedure similar to that described above for **3a**.

$[Et_4N][Nb(SCH{=}CHS)_3]$ (3b). The reaction system $NbCl_5$ (2.0 g, 7.4 mmol), LiSCH=CHSLi (2.5 g, 23.6 mmol), and Et_4NCl (1.24 g, 7.5 mmol) in CH_3CN/CH_2Cl_2 gave **3b** as a deep dull purple crystalline powder (yield 33%); mp 176–188 °C dec. ^1H NMR (DMSO-d_6, 100 MHz): δ 7.72 (s, 6 H, $SCH{=}CHS$), 3.22 (q, J = 7 Hz, 8 H, NCH_2CH_3), 1.16 (tt, J_{HH} = 7 Hz, 12 H, NCH_2CH_3). UV–visible (λ_{max}, nm (ϵ, M^{-1} cm^{-1}), CH_3CN): 317 (1000), 411 (2000), 460 (1700), 556 (1800). Anal. Calcd for $C_{14}H_{26}NS_6Nb$: C, 34.06; H, 5.32; N, 2.84; S, 38.96; Nb, 18.82. Found: C, 33.73; H, 5.23; N, 2.81; S, 38.34; Nb, 19.05.

$[Et_4N][Ta(SCH{=}CHS)_3]$ (4). The reaction system $TaCl_5$ (1.7 g, 4.7 mmol), LiSCH=CHSLi (1.8 g, 17.3 mmol), and Et_4NCl (0.78 g, 4.7 mmol) in CH_3CN/CH_2Cl_2 gave **4** as dark orange-red thin needlelike crystals upon recrystallization from CH_2Cl_2 (yield 36%); mp 153–174 °C dec. ^1H NMR (DMSO-d_6, 100 MHz): δ 7.96 (s, 6 H, $SCH{=}CHS$), 3.32 (q, J = 7 Hz, 8 H, NCH_2CH_3), 1.16 (tt, J_{HH} = 7 Hz, 12 H, NCH_2CH_3). UV–visible (λ_{max}, nm (ϵ, M^{-1} cm^{-1}), CH_3CN): 287 (3900), 371 (6100), 419 (4200), 493 (4500). Anal. Calcd for $C_{14}H_{26}NS_6Ta$: C, 28.90; H, 4.51; N, 2.41; S, 33.07; Ta, 31.11. Found: C, 28.51; H, 4.35; N, 2.73; S, 32.89; Ta, 31.61.

Syntheses of $[Et_4N][M(SCH_2CH_2S)_3]$ (M = Nb (**5b**), Ta (**6b**)) have been reported.[1b] The corresponding Ph_4P^+ salts were prepared by practically the same method with Ph_4PBr in place of Et_4NCl. Recrystallization from DMF gave the products, which are solvated by DMF.

$[Ph_4P][Nb(SCH_2CH_2S)_3]\cdot DMF$ (5a). The reaction system $NbCl_5$ (6.8 g, 25 mmol), $LiSCH_2CH_2SLi$ (8.2 g, 78 mmol), and Ph_4PBr (9.6 g, 23 mmol) in CH_3CN gave a deep red crystalline powder, which was recrystallized from DMF to give **5a** as deep red crystals (yield 77%), mp 156 °C dec. ^1H NMR (DMSO-d_6, 100 MHz): δ 8.0 (br, 1 H, $(CH_3)_2NCOH$), 7.8 (m, 20 H, Ph_4P), 3.66 (s, 12 H, SCH_2CH_2S), 2.92

(4) Examples of ethane-1,2-dithiolate complexes are as follows: (a) Dorfman, J. R.; Holm, R. H. *Inorg. Chem.* **1983**, *22*, 3179–3181. Dorfman, J. R.; Rao, Ch. P.; Holm, R. H. *Inorg. Chem.* **1985**, *24*, 453–454. Rao, Ch. P.; Dorfman, J. R.; Holm, R. H. *Inorg. Chem.* **1986**, *25*, 428–439. (b) Snow, M. R.; Ibers, J. A. *Inorg. Chem.* **1973**, *12*, 249–254. (c) Herskovitz, T.; DePamphilis, B. V.; Gillum, W. O.; Holm, R. H. *Inorg. Chem.* **1975**, *14*, 1426–1428. (d) Money, J. K.; Huffman, J. C.; Christou, G. *J. Am. Chem. Soc.* **1987**, *109*, 2210–2211; *Inorg. Chem.* **1985**, *24*, 3297–3302; **1988**, *27*, 507–514. Nicholson, J. R.; Huffman, J. C.; Ho, D.; Christou, G. *Inorg. Chem.* **1986**, *25*, 4072–4074. (e) Szeymies, D.; Krebs, B.; Henkel, G. *Angew. Chem.* **1984**, *96*, 797–798; *Angew. Chem., Int. Ed. Engl.* **1984**, *23*, 804–805. Tremel, W.; Krebs, B.; Henkel, G. *J. Chem. Soc., Chem. Commun.* **1986**, 1527–1529. (f) Blower, P. J.; Dilworth, J. R.; Hutchinson, J. P.; Zubieta, J. A. *Inorg. Chim. Acta* **1982**, *65*, L225–L226. Dahlstrom, P. L.; Kumar, S.; Zubieta, J. *J. Chem. Soc., Chem. Commun.* **1981**, 411–412. (g) Rakowski DuBois, M.; Haltiwanger, R. C.; Miller, D. J.; Glatzmaier, G. *J. Am. Chem. Soc.* **1979**, *101*, 5245–5252. (h) Pan, W.-H.; Chandler, T.; Enemark, J. H.; Stiefel, E. J. *Inorg. Chem.* **1984**, *23*, 4265–4269. Halbert, T. R.; McGauley, K.; Pan, W.-H.; Czernuszewicz, R. S.; Stiefel, E. I. *J. Am. Chem. Soc.* **1984**, *106*, 1849–1851.

(5) Schroth, W.; Peschel, J. *Chimia* **1964**, *18*, 171–173.

(d, 6 H, $(CH_3)_2NCOH$). UV-visible (λ_{max}, nm (ϵ, M^{-1} cm^{-1}), CH_3CN): 325 (11 000), 386 (10 000), 523 (4800). Anal. Calcd for $C_{33}H_{39}NOPS_6Nb$: C, 50.68; H, 5.04; N, 1.79; S, 24.60. Found: C, 50.61; H, 4.95; N, 1.84; S, 24.75.

$[Ph_4P][Ta(SCH_2CH_2S)_3]$·DMF (6a). The reaction system $TaCl_5$ (4.0 g, 12 mmol), $LiSCH_2CH_2SLi$ (4.2 g, 39 mmol), and Ph_4PBr (4.3 g, 10 mmol) in CH_3CN gave an orange crystalline powder from which **6a** was obtained upon recrystallization from DMF (yield 77%); mp 168 °C dec. ^1H NMR (DMSO-d_6, 100 MHz): δ 8.0 (br, 1 H, $(CH_3)_2NCOH$), 7.8 (m, 20 H, Ph_4P), 3.87 (s, 12 H, SCH_2CH_2S), 2.92 (d, 6 H, $(CH_3)_2NCOH$). UV-visible (CH_3CN): 291 (11 000), 332 (8900), 442 (4300). Anal. Calcd for $C_{33}H_{39}NOPS_6Ta$: C, 45.55; H, 4.53; N, 1.61; S, 22.11. Found: C, 45.31; H, 4.49; N, 1.64; S, 22.00.

X-ray Crystal Structure of 1a. Crystals of **1a** were obtained as described earlier in this section, and X-ray data were collected on a Philips PW1100 automated diffractometer as summarized in Table I; 25 centering reflections were used for determination of the lattice geometry and orientation. The data were corrected for Lorentz and polarization effects, but no absorption corrections were applied, for the crystal dimensions were reasonably uniform. Of 2256 observed reflections with $|F_o|^2 > 3.0\sigma(|F_o|^2)$, 2250 reflections were used in the final refinement.

The structure was solved with the SHELX-76 program[6,7] on a Melcom Cosmo 900II computer system (Osaka University). Examination of the systematic absences yielded two possible space groups, *Pn* (No. 7) and *P2/n* (No. 13). Simple *E* statistics favored the former noncentrosymmetric space group,[8] and successful full-matrix refinements of the structure based on the *Pn* group proved the choice to be correct. The structure was solved by using the standard Patterson heavy-atom method, which revealed the position of the Nb atom unequivocally. The remaining heavy atoms were located in succeeding difference Fourier syntheses. Most of the hydrogen atoms were observed in the difference maps, and they were included in the refinement along with the remaining poorly located hydrogen atoms, which were constrained to ride on the carbons to which they were bonded, with fixed isotropic thermal parameters. The C–H bond lengths were idealized at 0.97 Å. The phenyl rings of Ph_4P^+ were treated as semirigid bodies with C–C distances of 1.395 Å. In further refinements, all non-hydrogen atoms except for the phenyl rings were described anisotropically. A difference Fourier map after the final cycle of refinements showed two peaks of 2.2 e/Å^3 in the vicinity of the Nb atom; all other residual peaks were below 0.91 e/Å^3. The final *R* values and the weighting scheme used are given in Table I.

Other Physical Measurements. ^1H NMR spectra were recorded on a Varian XL-100 spectrometer. Infrared spectra were obtained on Jasco DS-402G and Hitachi FIS-3 spectrometers, while Raman spectra were measured on a Jasco R-800 spectrometer equipped with an NEC GLG 5800 He–Ne laser. For UV–visible spectra, a Jasco Uvidec-505 spectrometer was used. Electrochemical measurements were performed with the standard Yanaco P8-CV instrument, using a Pt working electrode, DMSO solvent (typically 4×10^{-3} M), and 0.1 M $(n\text{-}Bu_4N)(ClO_4)$ supporting electrolyte.

Molecular Orbital Calculations. All calculations were performed by using the extended Hückel method, with the weighted H_{ij} formula. The valence ionization potentials, H_{ii}, of Nb orbitals were determined by charge-iterative calculations on $[Nb(SCH_2CH_2S)_3]^-$ (θ = 16°). The other parameters were taken from previous works.[9]

The extended Hückel parameters are as follows. H_{ii}: Nb 5s, −9.41 eV; Nb 5p, −6.27 eV; Nb 4d, −11.1 eV; S 3s, −20.0 eV; S 3p, −13.3 eV; C 2s, −21.4 eV; C 2p, −11.4 eV; H 1s, −13.6 eV. Orbital exponents: Nb 5s, 1.89; Nb 5p, 1.85; Nb 4d, 4.08(0.6401) + 1.64(0.5516); S 3s, 3p, 1.817; C 2s, 2p, 1.625; H 1s, 1.30.

Assumed geometrical parameters are as follows. $[Nb(SCH_2CH_2S)_3]^-$: Nb–S = 2.43 Å; S–C = 1.82 Å; C–C = 1.50 Å; C–H = 1.09 Å. The CH_2–CH_2 portion is twisted by 20° to mimic the observed conformation. $[Nb(SCH{=}CHS)_3]^-$: Nb–S = 2.43 Å; S–C = 1.75 Å; C=C = 1.34 Å; C–H = 1.09 Å. The Nb–SCCS portion is planar.

Results and Discussion

Synthesis. Reaction of $NbCl_5$ with 3 equiv of dilithium propane-1,3-dithiolate in acetonitrile and the subsequent cation-exchange process with an acetonitrile solution of either PPh_4Br or Et_4NCl afforded the orange-red mononuclear propane-1,3-dithiolate complexes **1a** (43% yield) and **1b** (75%) upon recrystallization from dimethylformamide. The analogous Ta complexes

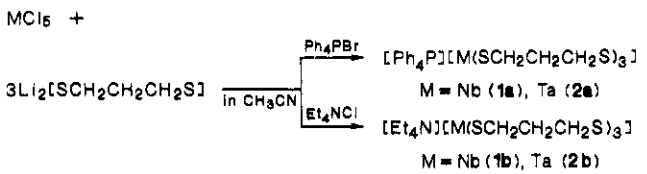

2a (75%) and **2b** (83%) were prepared in the $TaCl_5$/$LiSCH_2CH_2CH_2SLi$/PPh_4Br (or Et_4NCl) (1:3:1) reaction system, after workup similar to that for the Nb case, as yellow crystalline solids. All the complexes are moderately air and/or moisture sensitive, and those with the tetraethylammonium cation exhibit hygroscopicity. According to the room-temperature ^1H NMR spectra of **1a,b** and **2a,b**, the three propane-1,3-dithiolate ligands in the complexes are equivalent in solution. For instance, the spectrum of **1a** in $CDCl_3$ shows a single set containing a triplet (3.47 ppm) and a quintet (1.79 ppm) of relative intensity 2:1, in addition to the Ph_4P^+ signals. The triplet arising from the methylene group adjacent to sulfur is slightly shifted downfield (3.83 ppm) for the Ta congener **2a**. An analogous downfield shift of the ethanedithiolate proton signal (singlet) was noticed for $[Ph_4P][M(SCH_2CH_2S)_3]$ (M = Nb (**5a**), Ta (**6a**))[10] and $[Et_4N][M(SCH_2CH_2S)_3]$ (M = Nb (**5b**), Ta (**6b**))[1b] as well.

Similar to the preparation of **1a,b** and **2a,b**, mixing $NbCl_5$ or $TaCl_5$ with 3 equiv of dilithium ethylene-1,2-dithiolate in acetonitrile followed by reaction with PPh_4Br or Et_4NCl in dichloromethane and recrystallization from acetonitrile or dichloromethane gave a series of homoleptic ethylene-1,2-dithiolate complexes, **3a,b** and **4**, as deep dull purple (Nb) and orange-red (Ta) crystalline solids in 33–39% yields. Analytical and spectroscopic data are

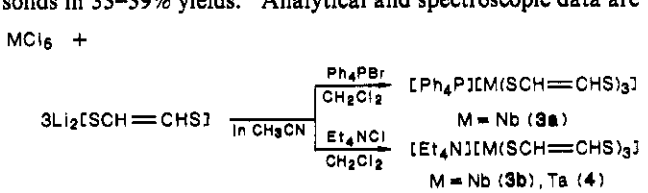

consistent with the formulas of **3a,b** and **4** as mononuclear diamagnetic species containing three ethylene-1,2-dithiolate ligands.

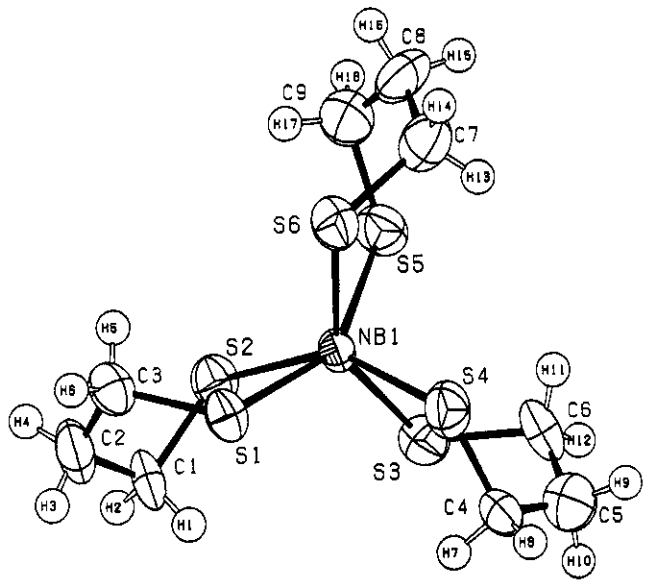

Figure 1. Molecular structure and atom-labeling scheme for the anion $[Nb(SCH_2CH_2CH_2S)_3]^-$ of **1a**.

(6) Sheldrick, G. M. "SHELX-76: Program for Crystal Structure Determination"; University of Cambridge: Cambridge, England, 1976.
(7) The atomic scattering factors and anomalous dispersion corrections for Nb were taken from: Cromer, D. T.; Mann, J. B. *Acta Crystallogr.* **1968**, *A24*, 321–324. Cromer, D. T.; Liberman, D. *J. Chem. Phys.* **1970**, *53*, 1891–1898.
(8) *E* statistics ($\langle|E^2-1|\rangle$ calculated as a function of sin θ are 0.612–0.726 when "unobserved" reflections are absent.
(9) (a) Basch, H.; Gray, H. B. *Theor. Chim. Acta* **1966**, *4*, 367–376. (b) Tatsumi, K.; Hoffmann, R. *J. Am. Chem. Soc.* **1981**, *103*, 3328–3341 and references therein.
(10) The phosphonium salts **5a** and **6a** were obtained by a procedure similar to the previously reported synthesis of **5b** and **6b**. See the Experimental Section.

Table II. Positional Parameters for **1a**

atom	*x*	*y*	*z*	*U*(eq), Å²
Nb	0.50 (0)	0.3442 (1)	0.50 (0)	0.037
S1	0.4733 (3)	0.1444 (3)	0.3840 (3)	0.051
S2	0.5369 (3)	0.1658 (4)	0.6309 (3)	0.053
S3	0.3915 (3)	0.4204 (4)	0.6346 (4)	0.060
S4	0.3845 (3)	0.4540 (4)	0.3802 (4)	0.064
S5	0.6066 (3)	0.4843 (4)	0.6094 (4)	0.064
S6	0.6065 (3)	0.4071 (4)	0.3600 (3)	0.059
C1	0.467 (1)	0.012 (1)	0.601 (1)	0.063
C2	0.515 (2)	−0.077 (1)	0.512 (2)	0.078
C3	0.552 (1)	0.007 (1)	0.427 (1)	0.052
C4	0.269 (1)	0.471 (2)	0.437 (2)	0.073
C5	0.261 (2)	0.579 (2)	0.519 (2)	0.095
C6	0.348 (1)	0.587 (2)	0.596 (2)	0.076
C7	0.648 (1)	0.583 (2)	0.383 (2)	0.074
C8	0.729 (1)	0.597 (2)	0.464 (2)	0.089
C9	0.724 (1)	0.499 (2)	0.552 (2)	0.077
P1	0.0677 (2)	−0.0136 (3)	0.5655 (3)	0.042
C12	0.2137 (6)	0.1192 (8)	0.6749 (7)	0.058
C13	0.2860 (6)	0.1293 (8)	0.7512 (7)	0.062
C14	0.3115 (6)	0.0147 (8)	0.8112 (7)	0.060
C15	0.2647 (6)	−0.1100 (8)	0.7950 (7)	0.052
C16	0.1924 (6)	−0.1201 (8)	0.7187 (7)	0.046
C11	0.1668 (6)	−0.0055 (8)	0.6587 (7)	0.044
C22	0.0484 (6)	−0.2303 (8)	0.4249 (6)	0.052
C23	0.0247 (6)	−0.3650 (8)	0.3978 (6)	0.056
C24	−0.0088 (6)	−0.4547 (8)	0.4736 (6)	0.066
C25	−0.0186 (6)	−0.4097 (8)	0.5766 (6)	0.051
C26	0.0051 (6)	−0.2749 (8)	0.6038 (6)	0.050
C21	0.0386 (6)	−0.1852 (8)	0.5279 (6)	0.042
C32	0.1923 (5)	0.0667 (9)	0.4133 (7)	0.055
C33	0.2185 (5)	0.1369 (9)	0.3232 (7)	0.056
C34	0.1533 (5)	0.2217 (9)	0.2706 (7)	0.056
C35	0.0619 (5)	0.2363 (9)	0.3081 (7)	0.059
C36	0.0357 (5)	0.1661 (9)	0.3982 (7)	0.053
C31	0.1009 (5)	0.0813 (9)	0.4508 (7)	0.047
C42	−0.1249 (6)	0.0125 (8)	0.5899 (7)	0.054
C43	−0.2065 (6)	0.0756 (8)	0.6261 (7)	0.069
C44	−0.1991 (6)	0.1899 (8)	0.6918 (7)	0.071
C45	−0.1100 (6)	0.2411 (8)	0.7212 (7)	0.066
C46	−0.0284 (6)	0.1780 (8)	0.6849 (7)	0.060
C41	−0.0359 (6)	0.0637 (8)	0.6193 (7)	0.052

The room-temperature ^{1}H NMR spectra exhibit one singlet for the olefinic protons, and a slight downfield shift of the peak was again observed in going from Nb (**3b**, 7.72 ppm) to Ta (**4**, 7.96 ppm).

X-ray Crystallography for Complex 1a. Crystal data are summarized in Table I, and a listing of fractional coordinates is presented in Table II, while selected interatomic distances and angles are given in Table III. The crystal structure of **1a** consists of discrete $[Ph_4P]^+$ cations and $[Nb(SCH_2CH_2CH_2S)_3]^-$ anions. A perspective view of the anion is shown in Figure 1, along with the numbering scheme adopted.

The $[Nb(SCH_2CH_2CH_2S)_3]^-$ anion represents a three-bladed propeller structure, at the center of which the niobium(V) atom is coordinated to six sulfur atoms in a distorted-octahedral (or a distorted-trigonal-prismatic) array. Coordination of a dithiolate ligand occurs with a twist-boat conformation, and the three NbS_2C_3 rings wring to the same direction. Thus, the complex anion possesses a pseudo-D_3 symmetry as incarnated in the distinct coplanarity of Nb, C2, C5, and C8, where the largest deviation from the least-squares plane is merely 0.07 Å. The degree of ring twist may be measured by the dihedral angles between the planes defined by S–Nb–S and C–C–C within the ligands. They are 44.1, 42.2, and 42.9°. A similar twist-boat MS_2C_3 conformation was found in the structure of $MoO(SCH_2CH_2CH_2S)_2$.[11]

The Nb–S bond lengths of 2.442 (4)–2.466 (4) Å fall in the range of normal Nb(V)–thiolate distances,[1b,c,12] while the average distance of 2.450 Å is somewhat longer than that found in $[Et_4N][Nb(SCH_2CH_2S)_3]$ (2.434 Å). Interestingly the mean Nb–S distance of the related benzenedithiolate complex $[Ph_4As][Nb(S_2C_6H_4)_3]$ (2.441 Å)[2c] lies between them, although one might anticipate that the π donor ability of the S atoms in $S_2C_6H_4$ would differ from that in the alkanedithiolate ligands because of delocalization of π electrons and could result in different Nb–S bond lengths. The S–Nb–S chelate bite angles range from 82.9 (1) to 84.0 (2)°, and the Nb–S–C angles are 107.4 (7)–112.3 (6)°. The average S–Nb–S bite angle of 83.5° is slightly but distinctively larger than the corresponding angles for $[Et_4N][Nb(SCH_2CH_2S)_3]$ (81.90°) and $[Ph_4As][Nb(S_2C_6H_4)_3]$ (80.35°). The mean Nb–S–C angle of **1a** (109.7°) is also slightly larger than those of the last two complexes (106.2 and 105.9°). Opening up of the S–Nb–S (intraligand) and Nb–S–C angles could simply be ascribable to the elongation of the bridging methylene chain.

Table III. Selected Interatomic Distances (Å) and Bond Angles (deg)

Nb–S1	2.466 (4)	C6–C5	1.55 (3)
Nb–S2	2.455 (4)	S3–C6	1.80 (2)
Nb–S3	2.445 (4)	S6–C7	1.83 (2)
Nb–S4	2.451 (4)	C7–C8	1.53 (3)
Nb–S5	2.442 (4)	C9–C8	1.48 (3)
Nb–S6	2.442 (4)	S5–C9	1.83 (2)
S2–C1	1.82 (2)	P1–C11	1.815 (8)
C1–C2	1.59 (3)	P1–C21	1.783 (8)
C3–C2	1.47 (2)	P1–C31	1.802 (8)
S1–C3	1.82 (1)	P1–C41	1.797 (9)
S4–C4	1.81 (2)		
C4–C5	1.50 (3)		
S2–Nb–S1	82.9 (1)	C3–C2–C1	113 (1)
S3–Nb–S1	124.9 (2)	C2–C3–S1	114 (1)
S3–Nb–S2	82.1 (1)	C5–C4–S4	116 (1)
S4–Nb–S1	83.2 (1)	C6–C5–C4	114 (1)
S4–Nb–S2	149.1 (2)	C5–C6–S3	113 (1)
S4–Nb–S3	83.5 (2)	C8–C7–S6	115 (1)
S5–Nb–S1	149.9 (2)	C9–C8–C7	114 (1)
S5–Nb–S2	83.7 (2)	C8–C9–S5	115 (1)
S5–Nb–S3	79.5 (2)	C21–P1–C11	112.6 (4)
S5–Nb–S4	120.2 (1)	C31–P1–C11	107.3 (4)
S6–Nb–S1	81.2 (1)	C31–P1–C21	109.0 (4)
S6–Nb–S2	123.4 (2)	C41–P1–C11	110.7 (4)
S6–Nb–S3	147.8 (1)	C41–P1–C21	108.1 (4)
S6–Nb–S4	81.2 (2)	C41–P1–C31	109.1 (4)
S6–Nb–S5	84.0 (2)	C12–C11–P1	119.3 (2)
C3–S1–Nb	108.7 (5)	C16–C11–P1	120.6 (2)
C1–S2–Nb	109.6 (6)	C22–C21–P1	121.3 (2)
C6–S3–Nb	107.4 (7)	C26–C21–P1	118.7 (2)
C4–S4–Nb	112.3 (6)	C32–C31–P1	119.2 (2)
C9–S5–Nb	111.3 (6)	C36–C31–P1	120.8 (2)
C7–S6–Nb	108.6 (7)	C42–C41–P1	119.0 (2)
C2–C1–S2	111 (1)	C46–C41–P1	120.9 (2)

As for the NbS_6 polyhedron of **1a**, the two triangular faces defined by S1, S4, S6 and S2, S3, S5 are nearly parallel, being tilted by only 0.4°. The Nb atom sits right in the middle of the two triangle centers, C_t and $C_{t'}$ and the C_t–Nb–$C_{t'}$ spine is linear (178.7°). The twist angle 2θ (Chart I) between the upper and lower triangular faces for each propane-1,3-dithiolate ligand is 17.3, 18.4, or 19.9°, with the average being 18.5°. They are closer to the trigonal-prismatic ideal of 0.0° rather than to the value of ca. 50° (θ = 25°) for the expected octahedral limit on the basis of the bidentate bite of b = 1.33[13] and lie between 0.7° (average) in $[Ph_4As][Nb(S_2C_6H_4)_3]$ and 30.5° (average) in $[Et_4N][Nb(SCH_2CH_2S)_3]$. The dihedral angles between the triangular S_3 faces and the three NbS_2 planes within the same ligand are 80.7, 79.8, and 77.9°, which also deviate somewhat from the trigonal-prismatic structure of 90°.

Octahedral vs Trigonal-Prismatic Structures in Terms of IR and Raman Spectra. We have analyzed the IR and Raman spectra of **1**–**4** as well as those of the previously reported tris(ethane-

(11) Bishop, P. T.; Dilworth, J. R.; Hutchinson, J.; Zubieta, J. A. *J. Chem. Soc., Chem. Commun.* **1982**, 1052–1053.

(12) The Nb–S distances in the diethyldithiocarbamate complex $[Nb(S_2CNEt_2)_4]Br$ are ca. 0.1 Å longer than those of **1a** and **5b**: Drew, M. G. B.; Rice, D. A.; Williams, D. M. *J. Chem. Soc., Dalton Trans.* **1985**, 1821–1828.

(13) Kepert, D. L. *Inorg. Chem.* **1972**, *11*, 1561–1563.

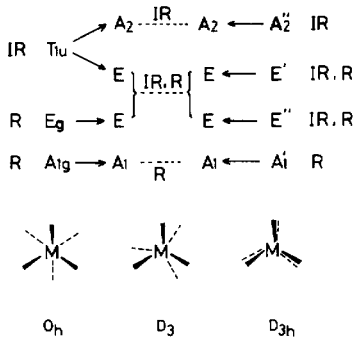

Figure 2. Schematic diagram of correlation between the stretching vibrational modes of O_h, D_3, and D_{3h} MS_6.

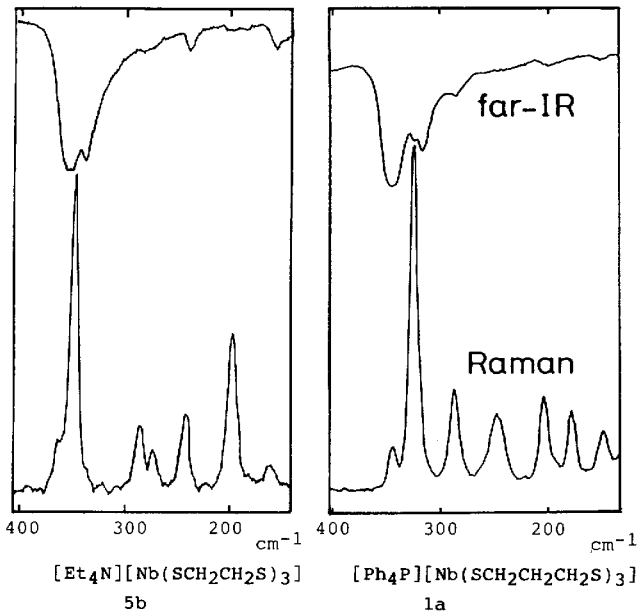

Figure 3. IR and Raman spectra in the 150–400-cm^{-1} region for **1a** and **5b**.

1,2-dithiolate) complexes of Nb and Ta **5** and **6**, in the hope that they could provide us with information about MS_6 coordination geometries. Our strategy is as follows: (1) to consider the bands arising from metal–sulfur vibrations at around 300–400 cm^{-1}, (2) to ignore chelation effects of the bidentate ligands on the spectra, if any, so that three bidentate ligands are thought to be equivalent to six monodentate thiolates, (3) to assume that there is no strong coupling between M–S and S–C stretching vibrations, and then (4) to assign peaks based on the simplified MS_6 skeleton model.

For an ideal octahedron there are three normal modes of stretching vibrations, A_{1g}, E_g, and T_{1u}, of which only T_{1u} is infrared active and the other two are Raman active. On the other hand, a trigonal-prismatic structure gives skeletal stretching vibrations of A_1', E', E'', and A_2'', while between the two limiting geometries normal modes for D_3 MS_6 consist of A_1, 2E, and A_2. Figure 2 illustrates the correlation between the stretching vibrational modes of the O_h, D_3, and D_{3h} MS_6 structures. It instructs us that the IR-active T_{1u} band splits into $A_2(A_2'')$ and $E(E')$ as the MS_6 unit twists from O_h to D_3 and to D_{3h} and that the A_{1g}–A_1–A_1' normal mode is Raman active regardless of geometry while the T_{1u}–A_2–A_2'' mode is kept IR active.

Figure 3 shows the typical far-IR and Raman spectra of $[Et_4N][Nb(SCH_2CH_2S)_3]$ (**5b**) and $[Ph_4P][Nb(SCH_2CH_2CH_2S)_3]$ (**1a**). For **5b**, the sharp Raman peak at 348 cm^{-1} can be assigned to the A_1 mode of the Nb–S stretching vibrations, while the two closely located IR bands at 354 and 338 cm^{-1} are determined to be the E and A_2 modes, which would be the degenerate T_{1u} if the molecule were in an ideal octahedral configuration. The spectra of **1a** give similar bands assignable to A_1, E, and A_2, and so do the other dithiolate complexes in hand. At the moment no attempt is made to assign another E band.

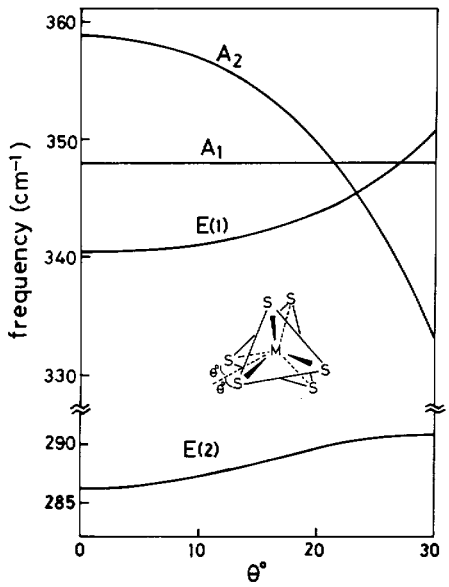

Figure 4. Calculated A_1, 2E, and A_2 frequencies as a function of θ based on the Urey–Bradley force field with b = 1.31, K^0 = 1.57 mdyn/Å, and F = 0.22 mdyn/Å.

Taking advantage of the fact that the M–S stretching vibrations are well isolated from the other stretching modes in the molecules, we performed a vibrational analysis based on the **GF** matrix method in order to elucidate how the M–S vibrational frequencies vary upon the trigonal twist of the MS_6 skeleton. As given in detail in the Appendix, the eigenvalues of **GF** and thus the M–S vibrational frequencies can be described as functions of the structure parameters θ and b and the force constants K^0 and F when the **F** matrix is written on the basis of the Urey–Bradley force field.

Given the geometrical parameters θ = 15° and b = 1.31 for $[Et_4N][Nb(SCH_2CH_2S)_3]$ (**5b**), we estimated K^0 and F to be 1.57 and 0.22 mdyn/Å, respectively, by fitting the Raman A_1 and IR A_2 frequencies. Then with use of these K^0 and F values, the four frequencies (A_1, 2E, A_2) were calculated for $0° < \theta < 30°$. Note that the MS_6 polyhedron is a trigonal prism (D_{3h}) at θ = 0°, but an ideal octahedron cannot be obtained even at θ = 30°, for the bidentate bite angle is not 90° (i.e., $b \neq 2$) in this case. Figure 4 shows the result. At θ = 15° the two E frequencies are calculated to be 342 and 288 cm^{-1}, which compare well with the observed IR band at 338 cm^{-1} and the Raman band at 285 cm^{-1}. Considering the approximate nature of our vibrational analysis, we cannot reproduce the observed frequencies very accurately. Nevertheless, the reasonable agreement encourages us in our further analysis.

According to Figure 4, the A_2 frequency is calculated to be higher than the E(1) frequency in the region $\theta < 24°$. Interestingly the angle θ = 24°, at which the accidental degeneracy takes place between A_2 and E(1), is close to the expected octahedral limit of ca. 25° for the bidentate bite b = 1.31. One conclusion to be drawn from the figure is that the gap between the A_2 and E(1) bands increases as θ decreases, provided that the far-right-hand side of Figure 4 ($\theta > 24°$) is geometrically unrealistic and is left out of consideration. By an analogous procedure with θ = 9° and b = 1.33 for $[Ph_4P][Nb(SCH_2CH_2CH_2S)_3]$ (**1a**), K^0 and F were determined to be 1.40 and 0.19 mdyn/Å, and then a band profile very similar to that of Figure 4 was obtained. The calculated A_2–E(1) gaps are 12 cm^{-1} for **5b** (θ = 15°) and 18 cm^{-1} for **1a** (θ = 9°). Although they are somewhat smaller than the observed values, being 16 and 28 cm^{-1}, respectively, the size of the gap may be a convenient measure of the trigonal twist of the MS_6 polyhedron: the larger the gap, the more MS_6 distorts toward a trigonal-prismatic structure.

The observed A_2–E(1) gaps for the 10 dithiolate complexes of Nb and Ta are summarized in the first column of Table IV. In the case of the ethanedithiolate complexes, those with Ph_4P^+ that happen to be solvated by DMF in the solid exhibit larger gaps compared with those in the corresponding Et_4N^+ complexes. The

Table IV. Gaps between the IR A_2 and E(1) Bands and Raman A_1 Frequencies

complex	$\Delta(A_2\text{–}E(1))$, cm^{-1}	A_1, cm^{-1}
$[Ph_4P][Nb(SCH_2CH_2S)_3]\cdot DMF$ (**5a**)	23	344
$[Et_4N][Nb(SCH_2CH_2S)_3]$ (**5b**)	16	348
$[Ph_4P][Nb(SCH_2CH_2CH_2S)_3]$ (**1a**)	28	325
$[Et_4N][Nb(SCH_2CH_2CH_2S)_3]$ (**1b**)	30	327
$[Et_4N][Nb(SCH{=}CHS)_3]$ (**3b**)	49	346
$[Ph_4P][Ta(SCH_2CH_2S)_3]\cdot DMF$ (**6a**)	26	354
$[Et_4N][Ta(SCH_2CH_2S)_3]$ (**6b**)	17	357
$[Ph_4P][Ta(SCH_2CH_2CH_2S)_3]$ (**2a**)	8	338
$[Et_4N][Ta(SCH_2CH_2CH_2S)_3]$ (**2b**)	7	342
$[Et_4N][Ta(SCH{=}CHS)_3]$ (**4**)	47	352

Table V. Half-Wave Potentials (V vs SCE) for Reduction of $[M(SCH_2CH_2S)_3]^-$,[a] $[M(SCH_2CH_2CH_2S)_3]^-$,[b] and $[M(SCH{=}CHS)_3]^-$[a] (M = Nb, Ta)[c]

ligand	metal		shift
	Nb	Ta	
SCH_2CH_2S	−1.20	−1.56	0.36
$SCH_2CH_2CH_2S$	−1.25	−1.59	0.34
$SCH{=}CHS$	−0.87	−1.04	0.17

[a] The Et_4N^+ salts. [b] The Ph_4P^+ salts. [c] See the Experimental Section for details.

presence or absence of the crystal solvent may be a reason behind the distinction, because no such difference is seen between $[Ph_4P][M(SCH_2CH_2CH_2S)_3]$ and $[Et_4N][M(SCH_2CH_2CH_2S)_3]$ for either M = Nb or M = Ta, all of which are unsolvated. On the other hand, the A_2–E(1) gap of the propanedithiolate complexes decreases notably on going from Nb to Ta, while for ethanedithiolate complexes the gap is hardly affected by a change of the metal. Thus, the solid-state geometry of these dithiolate complexes appears to vary in a complicated way depending on the minute perturbation of crystal-packing forces and electronic energies, and the adoption of a particular twist angle is likely to be determined by a delicate balance of these factors.

One noticeable trend seen in Table IV is the large A_2–E(1) gaps of $[Et_4N][M(SCH{=}CHS)_3]$, indicating that the molecular geometry is a trigonal prism or is close to it. This observation is not surprising because the majority of the related d^0 tris(dithiolene) complexes prefer prismatic coordination,[2,14,16] and such a geometrical choice has been explained in terms of the optimal overlaps between sulfur π orbitals and metal vacant d orbitals.[14b]

The second column of Table IV shows the observed Raman A_1 frequencies. Whether the cation is Ph_4P^+ or Et_4N^+, the ethanedithiolate complex of either Nb or Ta tends to have an A_1 frequency larger than that of the corresponding propanedithiolate complex. The calculated force constant K^0 follows the same trend; e.g., $[Et_4N][Nb(SCH_2CH_2S)_3]$ (1.57 mdyn/Å) > $[Ph_4P][Nb(SCH_2CH_2CH_2S)]$ (1.40 mdyn/Å). So it seems that ethanedithiolate is bound to the metal more strongly, which in fact parallels the order of the observed Nb–S bond lengths of **1a** and **5b**.

Chart II

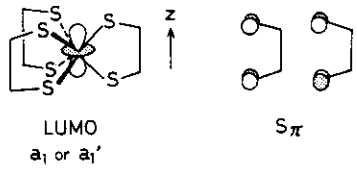

Electronic Properties. We have studied the redox properties of complexes **1–5** using the cyclic voltammetric technique. For each complex a single well-defined redox response at −0.87 to −1.59 V ($E_{1/2}$ vs SCE) was observed, and this was reversible. This process corresponds to a reduction of the anionic portion of **1–5**, and as one would anticipate, the identity of the countercation (Ph_4P^+ or Et_4N^+) has a negligible effect on the reduction potential. The results are summarized in Table V.

In the reduction process of the M(V)/M(IV) couple, one-electron transfer occurs probably to the lowest vacant M d level having $a_1(a_1')$ symmetry in the $D_3(D_{3h})$ point group.[14c,17,18] It follows from Table V that all the Ta complexes exhibit negative shifts of the reduction potentials relative to those of the Nb congeners, implying higher positioning of the Ta d energy level. This observation agrees with the trend of half-wave reduction potentials of $[Ph_4As][M(S_2C_6H_4)_3]$ (M = Nb, Ta) and is consistent with the idea that 5d orbitals of the third-row transition elements are higher in energy than 4d orbitals of the second-row transition series.

The reduction potential of $[Nb(SCH_2CH_2S)_3]^-$ is very similar to that of $[Nb(SCH_2CH_2CH_2S)_3]^-$, and the amounts of their negative shifts from Nb to Ta are essentially identical, suggesting structural and electronic similarity in solution among these alkanedithiolate complexes. This contrasts with geometrical diversity with a varying twist angle in the solid state that was noted by the X-ray analyses and by the Raman/IR spectra. The situation is different in the case of the ethylenedithiolate complexes. Their reduction potentials are much less negative and the Nb to Ta shift is also smaller. An obvious difference between alkanedithiolate and ethylenedithiolate is that in the latter ligand π electrons may delocalize over the sulfur and the carbon atoms. However, interpretation of the less negative reduction potential based on the π delocalization is not very straightforward as is discussed below.

We have performed extended Hückel calculations on $[Nb(SCH_2CH_2S)_3]^-$ and $[Nb(SCH{=}CHS)_3]^-$ using the computational and geometrical parameters given in the Experimental Section. For both complexes the LUMO, being assigned to $a_1(D_3)$ or to $a_1'(D_{3h})$, consists of mostly metal z^2 (see Chart II). The nature of the LUMO is the same as that obtained previously by other workers for various trigonally twisted ML_6 molecules.[14b,17] In D_{3h} ($\theta = 0°$), this orbital evidently does not overlap with any of the S π derived ligand orbitals due to the symmetry restriction. Therefore, delocalization of π electrons of ethylenedithiolate, which perturbs the sulfur π orbitals, does not affect the LUMO level through orbital interactions. On the other hand, we found that the trigonal twist of $[Nb(SCH_2CH_2S)_3]^-$ raised the LUMO energy slightly from −10.1 eV ($\theta = 0°$) to −9.7 eV ($\theta = 15°$). This is partly because the lowering molecular symmetry allows S π to interact with the LUMO and thereby pushes the energy level up. Considering the fact that the LUMO of D_{3h} $[Nb(SCH{=}CHS)_3]^-$ also lies at −10.1 eV, the observed negative shift of the reduction potential on going from $[Nb(SCH{=}CHS)_3]^-$ to $[Nb(SCH_2C-$

(14) (a) Smith, A. E.; Schrauzer, G. N.; Mayweg, V. P.; Heinrich, W. *J. Am. Chem. Soc.* **1965**, *87*, 5798–5799. Schrauzer, G. N.; Mayweg, V. P. *J. Am. Chem. Soc.* **1966**, *88*, 3235–3242. (b) Stiefel, E. I.; Eisenberg, R. C.; Rosenberg, R. C.; Gray, H. B. *J. Am. Chem. Soc.* **1966**, *88*, 2956–2966. (c) Eisenberg, R. *Prog. Inorg. Chem.* **1970**, *12*, 295. Wentworth, R. A. D. *Coord. Chem. Rev.* **1972**, *9*, 171. (d) The related tris(2-aminobenzenethiolato) complexes of Mo(VI) assume a trigonal-prismatic structure: Gardner, J. K.; Pariyadath, N.; Corbin, J. L.; Stiefel, E. I. *Inorg. Chem.* **1978**, *17*, 897–904. Yamanouchi, K.; Enemark, J. H. *Inorg. Chem.* **1978**, *17*, 2911–2917.

(15) There is a group of d^1, d^2 complexes with three bidentate ligands, geometries of which range from trigonal prism to octahedron: (a) Brown, G.; Stiefel, E. I. *Inorg. Chem.* **1973**, *12*, 2140–2147. (b) Draganjac, M.; Coucouvanis, D. *J. Am. Chem. Soc.* **1983**, *105*, 139–140. (c) Boyde, S.; Garner, C. D. *J. Chem. Soc., Dalton Trans.* **1987**, 2267–2271. (d) Colmanet, S. F.; Williams, G. A. *J. Chem. Soc., Dalton Trans.* **1987**, 2305–2310. (e) Stiefel, E. I.; Dori, Z.; Gray, H. B. *J. Am. Chem. Soc.* **1967**, *89*, 3353–3354.

(16) The estimated A_2–E(1) band gaps for **1a** and **5b** are smaller than the observed gaps, and the discrepancy increases as θ decreases. Correction of the calculated values according to the observation yielded a gap of ca. 40 cm^{-1} at $\theta = 0°$.

(17) (a) Hoffmann, R.; Howell, J. M.; Rossi, A. R. *J. Am. Chem. Soc.* **1976**, *98*, 2484–2492 and references therein. (b) Kirchner, R. M.; Mealli, C.; Bailey, M.; Howe, N.; Torre, L. P.; Wilson, L. J.; Andrews, L. C.; Rose, N. J.; Lingafelter, E. C. *Coord. Chem. Rev.* **1987**, *77*, 89–163.

(18) (a) Comba, P.; Sargeson, A. M.; Engelhardt, L. M.; Harrowfield, J. M.; White, A. H.; Horn, E.; Snow, M. R. *Inorg. Chem.* **1985**, *24*, 2325–2327. (b) Green, J. C.; Kelly, M. R.; Grebenik, P. D.; Briant, C. E.; McEvoy, N. A.; Mingos, D. M. P. *J. Organomet. Chem.* **1982**, *228*, 239–247. (c) Larsen, E.; La Mar, G. N.; Wagner, B. E.; Parks, J. E.; Holm, R. H. *Inorg. Chem.* **1972**, *11*, 2652–2668.

Table VI. Hypsochromic Shifts of the Three Low-Energy Bands of the UV–Visible Spectra in Going from Nb to Ta

complex	shift, eV[a] band 1	band 2	band 3
$[Ph_4P][M(SCH_2CH_2S)_3]$	0.43	0.52	0.45
$[Et_4N][M(SCH_2CH_2S)_3]$	0.42	0.50	0.41
$[Ph_4P][M(SCH_2CH_2CH_2S)_3]$	*b*	0.47	0.48
$[Et_4N][M(SCH_2CH_2CH_2S)_3]$	*b*	0.46	0.49
$[Et_4N][M(SCH{=}CHS)_3]$	0.28	0.27	0.32

[a] Band 1 means the lowest energy band, band 2 the second lowest, and so on. [b] These bands are shoulders, and their accurate positions cannot be determined.

$H_2S)_3]^-$ may be a consequence of the difference in their geometries in solution.

Another important outcome of our calculations is that the negative charge on S is notably smaller for $[Nb(SCH{=}CHS)_3]^-$, being −0.21 e (θ = 0°) vs −0.35 e (θ = 15°) for $[Nb(SCH_2CH_2S)_3]^-$. Conversely Nb of the former complex is somewhat less positively charged than that of the latter; +0.35 e vs +0.44 e. Interestingly the polarographic data of $M(S_2C_2R_2)_3$ (M = Mo, W; R = CH_3, Ph, CF_3) showed the order of ease of M(VI) → M(V) reduction to be CH_3 < Ph < CF_3.[14b] The trend agrees with the order of electron-withdrawing strength of the substituents, and thus the stability of the reduced state would increase in the same order. This explanation may also be applied to our Nb and Ta systems in the sense that ethylenedithiolate ligands would accommodate the reduced Nb(IV) and Ta(IV) metal more easily due to the smaller negative charge on S that is primarily caused by π delocalization. The above argument is based on relative stability of the reduced state and has nothing to do with the M(V) oxidized-state properties.

We gave two plausible interpretations of the observed redox properties. At present it is difficult to conclude which of them is the dominant factor. It may be that both factors are operative.

In the UV–visible spectra of **1**–**6** in CH_3CN, the three low-energy absorption bands in the 290–560-nm range, assignable to sulfur → metal transitions, are instructive. As in the case of cyclic voltammograms, the choice of countercation hardly alters the spectral pattern. For either Nb or Ta, the three bands shift systematically to higher wavelengths on going from SCH_2CH_2S to $SCH_2CH_2CH_2S$ to SCH=CHS, except for the lowest band of the propanedithiolate complexes, which appears as a shoulder of the second lowest band and the location of which is not determined accurately. There, the difference between the first two ligands is moderate, while that between the last two is rather large. An intriguing aspect of the spectra is the nearly constant blue (hypsochromic) shift of the three bands with a change in the metal from Nb to Ta, as summarized in Table VI. This proves that the three bands arise from charge-transfer (sulfur → metal) transitions and that all the transitions occur to the same d level or to d levels of a similar type. The size of the blue shifts is similar between $[M(SCH_2CH_2S)_3]^-$ and $[M(SCH_2CH_2CH_2S)_3]^-$, while that for $[M(SCH{=}CHS)_3]^-$ is much smaller. This result correlates well with the behavior of reduction potentials in Table V.

Our molecular orbital calculations on $[Nb(SCH_2CH_2S)_3]^-$ and $[Nb(SCH{=}CHS)_3]^-$ give level diagrams similar to the one derived by Gray et al. for $Re(S_2C_2Ph_2)_3$.[14b] Therefore, there is not much to say here about the further assignments of the three low-energy bands. However, it is worth mentioning that the two highest occupied levels of largely ligand character, a_2' and e', move up in energy for $[Nb(SCH{=}CHS)_3]^-$ by 0.90 and 0.17 eV, respectively. This is caused by interactions between S π and olefin π orbitals and may explain the notable shifts of the bands to higher wavelengths.

Chart III

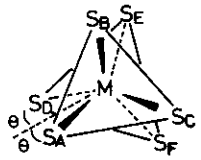

D_3 Symmetry

$\alpha = \angle S_A\text{-}M\text{-}S_B = \angle S_B\text{-}M\text{-}S_C = \angle S_C\text{-}M\text{-}S_A$
$\beta = \angle S_A\text{-}M\text{-}S_D = \angle S_B\text{-}M\text{-}S_E = \angle S_C\text{-}M\text{-}S_F$
$\gamma = \angle S_A\text{-}M\text{-}S_F = \angle S_B\text{-}M\text{-}S_D = \angle S_C\text{-}M\text{-}S_E$
$\delta = \angle S_A\text{-}M\text{-}S_E = \angle S_B\text{-}M\text{-}S_F = \angle S_C\text{-}M\text{-}S_D$

Acknowledgment. We are grateful to Dr. K. Tashiro (Osaka University) for helpful advice on the force-field analysis.

Appendix

Chart III illustrates the stereochemistry for D_3 MS_6, where the S–M–S angles, α–δ, may be written as in (1)–(4) by using half of the trigonal twist angle θ and the bidentate bite b according to the Kepert notation.[13] Note that the S_A–S_D, S_B–S_E, and S_C–S_F pairs represent the dithiolate ligands.

$$\cos\alpha = (2\cos^2\theta - 3 + {}^3/_4 b^2)/2\cos^2\theta \quad (1)$$

$$\cos\beta = 1 - b^2/2 \quad (2)$$

$$\cos\gamma = [-2\cos^2\theta + (4 - b^2)\cos^2(60° - \theta)]/2\cos^2\theta \quad (3)$$

$$\cos\delta = [-2\cos^2\theta + (4 - b^2)\cos^2(60° + \theta)]/2\cos^2\theta \quad (4)$$

If the stretch–bend interaction is ignored, the G matrix elements in terms of (internal) stretching coordinates of MS_6 with six equivalent M–S bonds are as in (5) and (6), where μ is the reduced

$$G_{ii} = \mu_M + \mu_S \quad (5)$$

$$G_{ij} = \mu_M \cos(\angle S_i\text{-}M\text{-}S_j) \quad (6)$$

$$S_i, S_j = S_A\text{-}S_F$$

mass.[19] Transformation of (5) and (6) into symmetry coordinates of the group D_3 results in (7)–(9). Substituting (1)–(4) into (7) shows A_1 to be equal to μ_S and thus to be independent of θ and b.

As for **F**, the complete generalized valence force field for the M–S stretches in D_3 MS_6 would require one diagonal force constant and four interaction constants. There are, however, four observed frequencies available at best, which are not sufficient to determine these force constants independently. Furthermore, even if the force constants were estimated, they would vary from one molecule to the other in a complicated fashion and they would not give us a clear picture showing the effect of a trigonal twist on the frequencies. Therefore, we decided to utilize the Urey–Bradley force field to describe **F**.[19a] The matrix elements in

$$\mathbf{G} = \begin{bmatrix} A_1 & \mu_S + \mu_M(1 + 2\cos\alpha + \cos\beta + \cos\gamma + \cos\delta) & (7) \\ E(1) \\ E(2) & 2\begin{pmatrix} \mu_S + \mu_M\left(1 - \cos\alpha - \frac{\sqrt{3}}{2}\cos\gamma + \frac{\sqrt{3}}{2}\cos\delta\right) & \mu_M\left(\cos\beta - \frac{1}{2}\cos\gamma - \frac{1}{2}\cos\delta\right) \\ \mu_M\left(\cos\beta - \frac{1}{2}\cos\gamma - \frac{1}{2}\cos\delta\right) & \mu_S + \mu_M\left(1 - \cos\alpha + \frac{\sqrt{3}}{2}\cos\gamma - \frac{\sqrt{3}}{2}\cos\delta\right) \end{pmatrix} & (8) \\ A_2 & \mu_S + \mu_M(1 + 2\cos\alpha - \cos\beta - \cos\gamma - \cos\delta) & (9) \end{bmatrix}$$

stretching coordinates are then

$$F_{ii} = K + \sum_{j}^{j \neq i} (t_{ij}^2 F' + s_{ij}^2 F) \quad (10)$$

$$F_{ij} = -t_{ij}^2 F' + s_{ij}^2 F \quad (11)$$

where s_{ij}^2 and t_{ij}^2 can be written as functions of θ and b as in (12)–(16) and the summation runs over all neighboring M–S bonds. The second term of the diagonal elements (10) becomes a constant, and we write F_{ii} as K^0. When F' is taken as $-1/10F$,[20] the off-diagonal elements are functions of θ, b, and F. The **F** matrix may be transformed to symmetry coordinates leading to the form analogous to (7)–(9), from which, combined with (7)–(9), the eigenvalues of **GF** may be calculated.

$$s_{S_AS_B}^2 = s_{S_AS_C}^2 = \left(3 - \frac{3}{4}b^2\right) \Big/ 4 \cos^2 \theta \quad (12)$$

$$s_{S_AS_D}^2 = b^2/4 \quad (13)$$

$$s_{S_AS_F}^2 = [4 \cos^2 \theta - (4 - b^2) \cos^2 (60° - \theta)]/4 \cos^2 \theta \quad (14)$$

$$s_{S_AS_E}^2 = [4 \cos^2 \theta - (4 - b^2) \cos^2 (60° + \theta)]/4 \cos^2 \theta \quad (15)$$

$$t_{ij}^2 = 1 - s_{ij}^2 \quad (16)$$

Supplementary Material Available: Complete listings of thermal parameters and hydrogen atom parameters for **1a** (3 pages); a listing of observed and calculated structure factors for **1a** (23 pages). Ordering information is given on any current masthead page.

(19) (a) Nakamoto, K. "Infrared Spectra of Inorganic and Coordination Compounds"; Wiley: New York, 1970. (b) Murrell, J. N. *J. Chem. Soc. A* **1969**, 297–301.

(20) This approximation assumes that the repulsive energy between nonbonded sulfur atoms is proportional to $1/r^9$.